Simulation of Synchronous Motors for Industrial Drives

[1]Iossif Grinbaum, [2]Cornelius Jäger and [2]Jasmin Smajic
[1]ABB Switzerland Ltd., Segelhofstrasse 9P, CH-5405 Baden-Dättwil, Switzerland
[2]University of Applied Sciences of Eastern Switzerland (HSR), Oberseestrasse 10, 8640 Rapperswil
E-mail: jasmin.smajic@hsr.ch

***Abstract*— the paper presents the numerical methods for computing synchronous motors with salient pole rotor without damper winding for industrial drives. Two possible regimes of the adjacent high power cycloconverter were modeled as an ideal current- and voltage harmonic source. The obtained results are important for understanding the behavior of the synchronous motor and the entire system in those two important converter regimes. The obtained results were verified by comparison between two different simulation tools based on essentially different simulation technologies and a very good agreement was found. It is demonstrated that the described methods can be effectively used in daily design and optimization of synchronous motors.**

***Index Terms*— Industrial drive, numerical methods, and synchronous motors with salient pole rotor.**

I. INTRODUCTION

Synchronous motors (SM) for industrial drives are very large due to their high torque and low speed requirements. The inner diameter of the stator of largest units reaches 15 meters and their power reaches today 30MW. The modern industrial drives are sometimes in operation in harsh environment at elevations higher than 2'000 meters above sea level. This requirement makes the dielectric, magnetic, mechanical, and thermal design of these motors rather demanding.

The motor as the most important component of the industrial drive can be designed by using the well- known analytical approach presented, for example, in [1], [2] and [4].

As an alternative to the mentioned analytical approach, it is possible to design the motor by using numerical field simulations to obtain the motor parameters. This method is also well-known and already reported for example in [1], [4], [5] and [6]. It is also worth mentioning here that the field simulation approach can be very detailed but therefore also costly in terms of CPU-time and memory requirements.

The numerical techniques for computing synchronous motors presented in [4], [5] and [6] are capable of dealing with complicated real-life geometries and of taking into account magnetic nonlinearities of the involved materials. The reference [4] presents the numerical analysis of large synchronous motors for industrial drives based on the extraction of the motor's leakage and armature reaction reactances from the obtained magnetic field distribution. Additionally, the paper [4] presents the dependence of the reactances from the magnetic saturation level of the stator and rotor magnetic circuit.

In contrast to the existing publications this paper presents in detail: (a) a simulation methodology (the voltage source approach - VSA) that couples the voltage equation of the stator circuit with the magnetic field equations of the field simulation initial boundary value problem (IBVP) relevant for the analysis of synchronous motors, (b) the current source simulation approach (CSA) based on the solely solution of the field simulation IBVP, and (c) the comparison of the two.

Those two different numerical methodologies are important for modeling and simulation of the two corresponding operating modes of the adjacent cycloconverter responsible for the power supply and control of the SM.

The paper is organized as follows. Section II describes the numerical methods for simulating synchronous motors for industrial drives. Section III presents the obtained results and their comparison. Section IV contains the results of a motor parameter study performed by using the suggested methods. Section V concludes the paper.

II. NUMERICAL METHODS

For the reasons of completeness it is worth starting this section with an accurate analytical description of a synchronous motor with salient pole rotor. The stator voltage equation written in frequency domain has the following form [7]:

$$\underline{U} = R\underline{I} + jX_\sigma \underline{I} + jX_{ad}\underline{I}_d + jX_{aq}\underline{I}_q + \underline{U}_p \tag{1}$$

where U is the stator terminal voltage, I is the stator current, I_d is the direct component of the stator current (the d-axis current component), I_q is the quadrature component of the stator current (the q-axis current component), U_p is the synchronous generated voltage of the stator winding induced by the rotor's rotating field, X_σ is the stator leakage reactance, X_{ad} is the d-axis armature reaction reactance, and X_{aq} is the q-axis armature reaction reactance. In addition to Equation (1) the following useful and important additional equations can be written [7], [4]:

$$\underline{I} = \underline{I}_d + \underline{I}_q \tag{2}$$

$$\underline{I}_\mu = \underline{I}_d + \underline{I}_q + \underline{I}_E \tag{3}$$

$$X_d = X_\sigma + X_{ad} \tag{4}$$

$$X_q = X_\sigma + X_{aq} \tag{5}$$

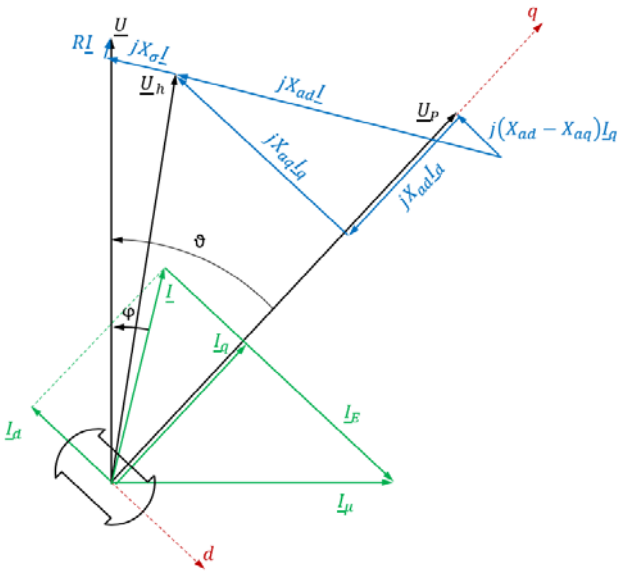

Figure 1: The vector diagram of the considered ABB synchronous motor with salient pole rotor (15.6MW, 3'900V, 5.6Hz) at the nominal operating point is presented.

where I_μ is the magnetizing current of the SM, I_E is the excitation rotor current recomputed to the stator winding, X_d is the d-axis synchronous reactance, and X_q is the q-axis synchronous reactance.

Equations (1)–(5) present the well-known two reactance theory (the d-q theory) of salient pole synchronous machine [6]. The meaning of the d-q theory and its parameters can be understood from the vector diagram of the SM with salient pole rotor shown in Figure 1. This theory is used to compute the motor current, torque and power for a given terminal voltage and load angle.

The d-q theory given by Equations (1)–(5) and by the vector diagram in Figure 1 is valid in frequency domain assuming that the currents and voltages of the model are harmonic sinusoidal time-functions.

The presented theory is a useful approximation of the SM but cannot accurately capture the effect of magnetic saturation and the effect of the motor's complicated geometric features such as winding slots, non-uniform thickness of the air gap, and non-sinusoidal distribution of the B-field in the air gap.

A more accurate approach based on magnetic field simulations is capable to accurately describe all the mentioned effects in the SM. This means, however, that a transient time-domain analysis is required since the B-field of the motor cannot be considered sinusoidal.

The initial boundary value problem (IBVP) of the transient time-domain magneto-quasistatic analysis of the SM has the following form [3], [5] and [6]:

$$-\frac{\partial}{\partial x}\left(\frac{1}{\mu}\frac{\partial A_z}{\partial x}\right)-\frac{\partial}{\partial y}\left(\frac{1}{\mu}\frac{\partial A_z}{\partial y}\right)+\sigma\frac{\partial A_z}{\partial t}=J_z \text{ , in } \Omega\subseteq R^2 \quad (6)$$

$$A_z(x,y,t)=0 \text{ , on } \partial_D\Omega \quad (7)$$

$$A_z(r,\theta_0+p,t)=-A_z(r,\theta_0,t) \text{ , on } \partial_P\Omega \quad (8)$$

$$A_z(x,y,t)=0 \text{ , for } t=0 \quad (9)$$

where A_z is the z-component of the magnetic vector potential perpendicular to the motor's cross section ($x0y$-plane), μ is the magnetic permeability of the material, J_z is the source current density (existing only in the winding regions), σ is the electric conductivity of the material, Ω is the computational domain (the cross section of the motor), $\partial_D\Omega$ is the Dirichlet's boundary with the known vector magnetic potential, and $\partial_P\Omega$ is the periodic boundary.

In the previous publication [4] the numerical method based on the IBVP (6)-(9) and its Finite Element Method (FEM) solution was suggested. The method published in [4] considered the coils "stranded", which means that no eddy currents in the windings were computed. Thus, the problem (6)–(9) becomes a magneto-static problem that is used to compute the B-field and the corresponding motor reactances (4) and (5) out of the magnetic field energy and magnetic flux for various saturation levels of the motor's magnetic circuit [4]. It has been shown that this method delivers accurate results.

In this paper, a numerical technique that should deliver even more accurate results is suggested, namely the coupling of the IBVP (6)–(9) with the following voltage balance equation of the stator circuit:

$$u(t)=R\cdot i(t)+L_{\sigma ew}\cdot\frac{di}{dt}(t)+u_{ind}(t) \quad (10)$$

where $L_{\sigma ew}$ is the stray inductance of the stator's end winding region, and u_{ind} is the total induced voltage of the stator winding due to the rotating magnetic flux, the stray magnetic flux and the armature reaction flux of the motor.

The coupling channel between the IBVP (6)-(9) and the voltage balance equation (10) is the induced voltage:

$$u_{ind}(t)=N\cdot\frac{\partial\Phi}{\partial t}(t)=N\cdot L\cdot\frac{1}{S}\frac{\partial}{\partial t}\iint_{(S)}A_z(x,y,t)\cdot dS \quad (11)$$

where N is the number of turns of the stator winding, L is the axial length of the motor, and S is the surface area of the stator coil covering all its slots.

Having the capability to solve the time-domain IBVP (6)-(9) by using the FEM [3] for any source current density function on the right hand side of Equation (6) the following iterative process is possible:

a. Starting from the zero initial condition (9) in the first time step or starting with the solution of the previous time step in all the subsequent steps, the A_z-field distribution after the next time step of the IBVP (6)-(9) for an anticipated/estimated value of the source current density should be computed.
b. Based on the solution (a) the induce voltage of the stator phase winding according to (11) should be computed.
c. The voltage error according to (10) should be estimated.
d. Based on the solution (c) the stator current according

to Equation (10) should be corrected.

e. If the current correction obtained in (d) is lower than the tolerable error the process has converged (the solution has been found) and if not the process goes to (a) but with the corrected current value.

The main assumption of this process is that the source voltage on the left hand side of Equation (10) is given and that the resistance R and inductance $L_{\sigma ew}$ are known. By knowing the winding structure the resistance can be easily calculated. From the geometry of the end winding region the inductance $L_{\sigma ew}$ can be analytically estimated [1].

The iterative process (a-e) is a basis of the first method suggested in the paper that is called "the voltage source approach (VSA)". For each load angle ϑ shown in Figure 1 between 0 and π that is set within the simulation model by geometrically placing the rotor at right position relative to the stator's rotating magnetic field, the corresponding current is computed according to the iterative process (a-e). In this process the rotor is rotating with the same synchronous speed of the stator's rotating field. The described VSA converges after a couple of voltage periods, as depicted in Figure 2c.

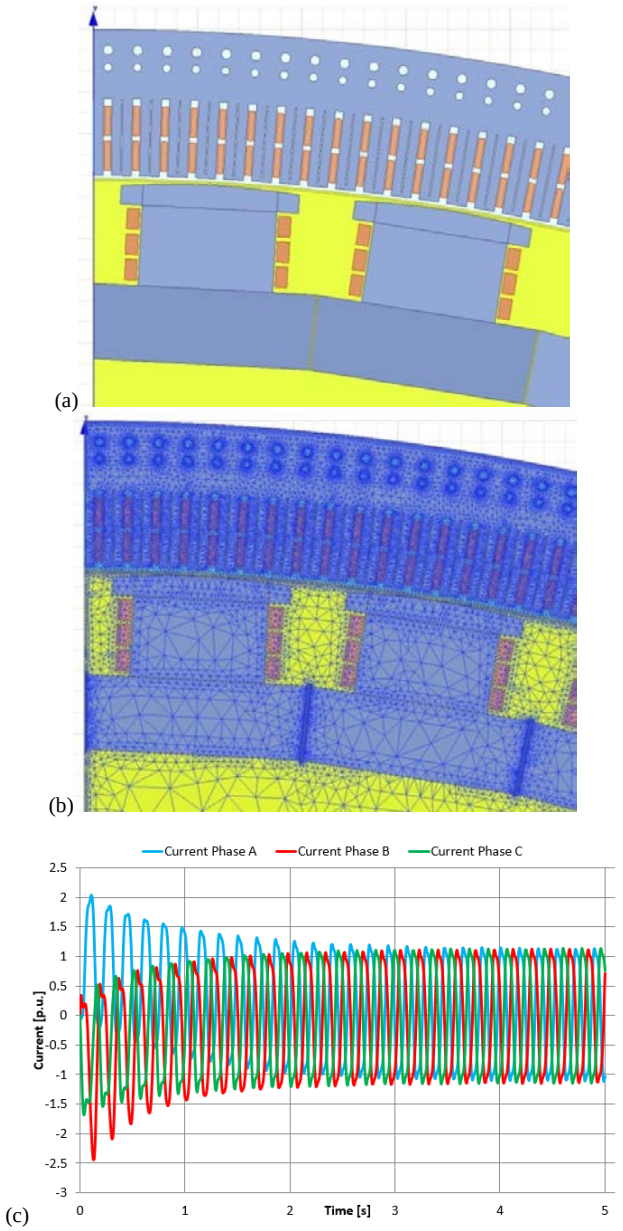

Figure 2: The geometry (a), FEM mesh (b) and the motor's currents over the transient solution process (c) by using the described VSA. A typical ABB synchronous motor with salient pole rotor (15.6MW, 3'900V, 5.6Hz) is considered.

In addition to the described VSA it is possible to define the so called "current source approach (CSA)". The main idea of the CSA is to set the motor current to a fixed sinusoidal time function and to perform field simulations for each value of the load angle defined by discretizing the segment from 0 to π with a certain desired resolution. The voltage in this case is a variable that can be computed for each value of the load angle. The CSA can be performed faster than the VSA. If the induced eddy currents in windings are to be neglected, it is recommended to fix the rotor position and solve the IBVP (6)-(9) for the time interval of one single turn. Thus, the field solution for each value of the load angle is computed. The resolution of the load angle discretization is then determined by the time step of the IBVP solution process.

After the field solution over the entire period of the source voltage (VSA) or the source current (CSA) is obtained, the motor torque can be computed as the time average value of the following function [5], [6]:

$$M(t) = \frac{\partial W_m}{\partial \vartheta}(t) \tag{12}$$

where W_m is the magnetic energy stored in the motor's magnetic field.

Equation (12) is not the only method for computing the torque. The torque can be also computed by integrating the magnetic Lorentz force acting on the rotor conductors [5], [6]:

$$\vec{f}_L(x,y,t) = \vec{J}(x,y,t) \times \vec{B}(x,y,t) \tag{13}$$

$$M(t) = L \cdot \iint_{(S_r)} \vec{r}(x,y) \times \vec{f}_L(x,y,t)\, dS \tag{14}$$

where f_L is the Lorentz force density, L is the length of the motor, r is the position vector of the current integration point relative to the rotational axis, S_r is the surface of the rotor conductors, J is the current density and B is the magnetic flux density.

The geometrical arrangement of a typical synchronous motor considered in this paper is presented in Figure 2a. The finite element mesh used to discretize and solve the IBVP (6)-(9) is also visualized (Figure 2b).

The obtained solution of the VSA in form of the stator phase currents is depicted in Figure 2c. This solution looks rather realistic for the following arguments. At the beginning of the transient solution algorithm the motor is attached to the three-phase grid voltage and the motor is not energized (the zero initial condition given by

Equation (9)). To reach the voltage equilibrium, i.e. to enter the stationary regime a certain time is needed. According to the result given in Figure 2c, the stationary regime is reached after the time of around 3 seconds. This is determined by the electromagnetic time constant of the motor and this constant can be obtained from this simulation result.

It is worth mentioning that this solution is obtained for a given load angle ϑ that is set at the beginning of the simulation by the geometrical position of the rotor relative to the stator's rotating field. After setting its initial geometrical position, the rotor rotates with the same synchronous speed as the rotating field of the stator over the entire simulation time.

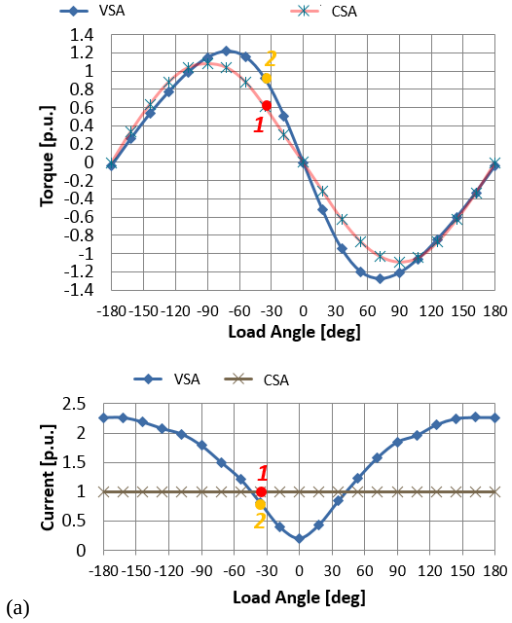

(a)

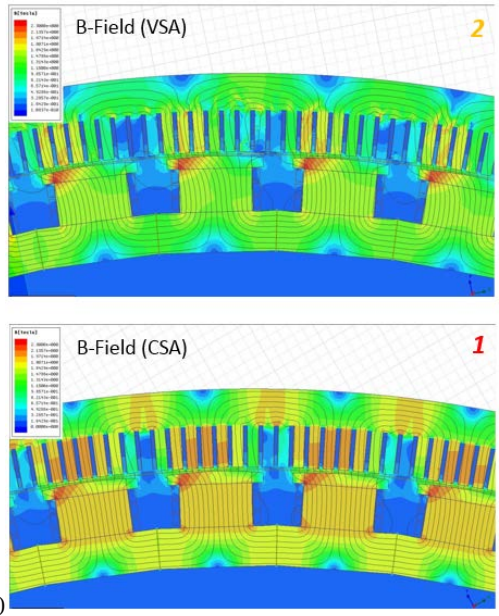

(b)

Figure 3: The obtained motor torque and stator current (a) by using the VSA and CSA are depicted. The magnetic flux density distribution at the nominal operating point (ϑ=36°) is shown (b). The chosen SM presented in Figure 2 was considered.

III. Numerical Results

The chosen SM presented in Figure 2 was simulated by using the described VSA and CSA. The obtained torque and stator current along with the B-field distribution in one operating point (ϑ=36°, motor regime) are presented in Figure 3.

The results presented in Figure 3 are obtained by using the transient time-domain field solver ANSYS Maxwell [7].

It is important to notice that the torque curve obtained by the CSA is almost sinusoidal and the VSA results deviate significantly from the sinusoidal curve. The VSA torque curve reaches also a higher breakdown torque. The result look so as the contribution of the reluctance torque to the total torque is much more significant in the voltage source regime (VSR) compared to the current source regime (CSR). This is confirmed by the Fourier analysis shown in Figure 5.

The measurements of the torque curve on such motors are not presently available due to the high costs of such experiments. Therefore a different strategy for verifying the numerical results was chosen.

The ANSYS Maxwell solves the IBVP (6)-(9) and computes the torque according to Equation (12). For verifying the obtained results the same motor was simulated by using the field solver MagNet of Infolytica [8]. The solver MagNet uses a different field formulation (the so-called *T-Ω* formulation) for solving the transient magnetic field and computes the torque according to Equation (14). Due to the essentially different simulation algorithms of the two field solvers for computing the magnetic field and torque, the comparison of their results can be used for a fair verification of the obtained results.

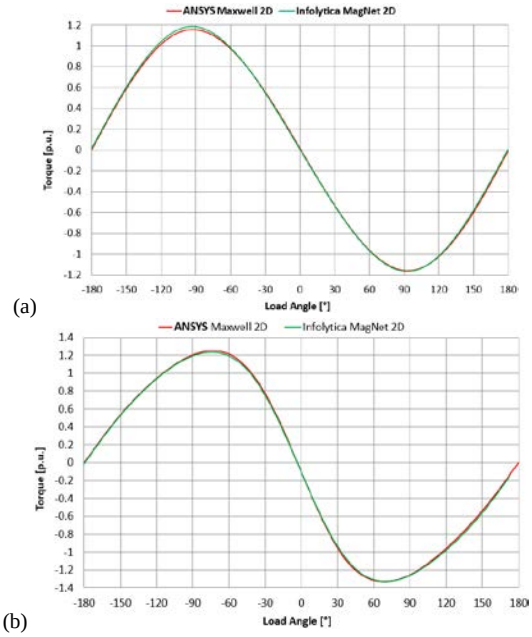

(a)

(b)

Figure 4: The obtained motor torque by using the CSA (a) and VSA (b) are depicted. The verification of the results by comparison between the ANSYS Maxwell and Infolytica MagNet is presented. The chosen SM presented in Figure 2 was considered.

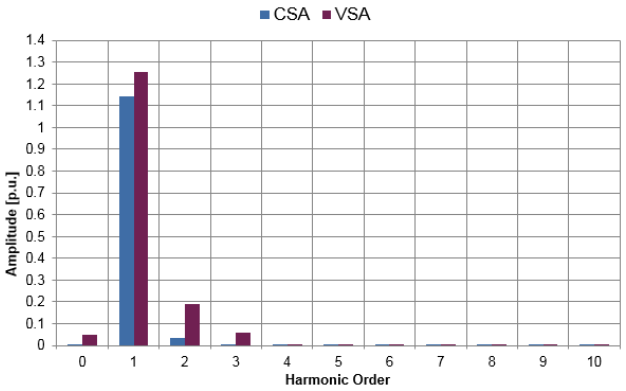

Figure 5: The Furrier analysis of the torque curves presented in Figure 4. The fundamental frequency of this analysis is 5.6Hz (the harmonic order 1).

The verification of the obtained results by comparison between the two field solvers is presented in Figure 4. Evidently, the agreement of the obtained results is excellent.

IV. Parametric Study

After the results of the suggested methods were verified, the described numerical techniques have been applied to a parametric study of the chosen motor. The main goal of the study is to analyze the influence of the pole shoe geometry on the motor performance. The problem definition and the obtained results are shown in Figure 6.

Evidently, the chosen variables influence significantly the breakdown torque of the motor. The reason for this are the higher harmonics of the B-field in the air gap, i.e. the deviation of the B-field distribution from the sinusoidal distribution along the air gap. This is determined mainly by the factor λ defined in Figure 6.

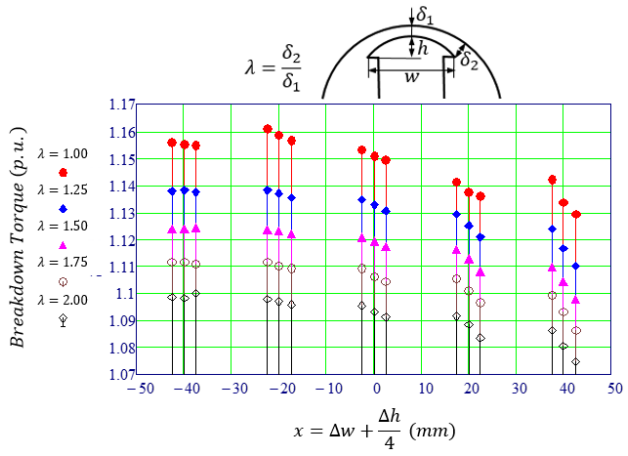

Figure 6: The variables of the parametric study, which determine the pole shoe geometry, are shown on the top of the picture. The obtained results in the form of the breakdown torque are presented. The width (5 steps) and height (3 steps) of the pole shoe was changed with a step of 20mm and of 10mm respectively. The height difference is divided by 4 so that the changes of the height for each change of the width produce a group with three designs.

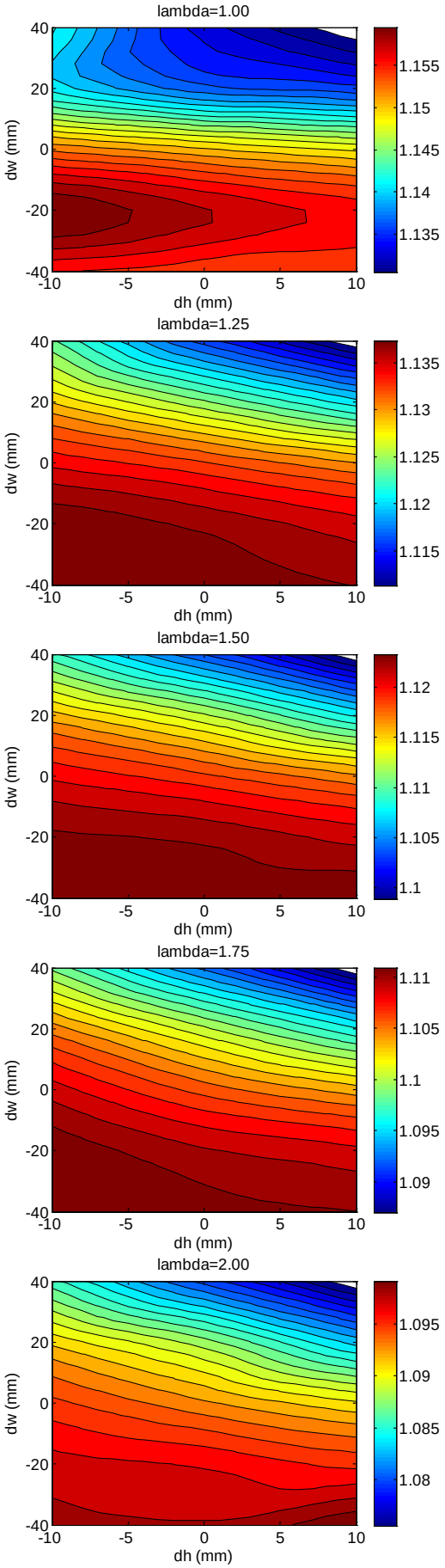

Figure 7: The breakdown torque of the chosen motor as a result of the parametric study defined in Figure 5 is depicted.

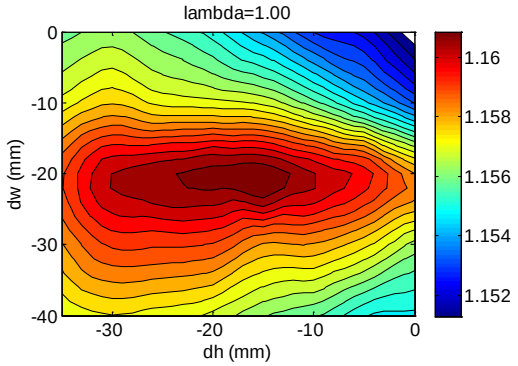

Figure 8: The behavior of the breakdown torque in the vicinity of the local optimum anticipated in the result of the parametric study sown in Figure 6 (λ =1.00) is depicted.

The results presented on the Figure 6 show the main advantage of applying FEM simulations for optimization of SMs.

Since the results presented in Figure 6 have a very compact form they are in detail presented in Figure 7. Such an information is essential for the designers as they reveal possibilities and direction of design improvement, i.e. design optimization.

The highest breakdown torque found during this study is ca. 4% bigger in comparison to the base design. To reach this solution width of the pole shoe should be reduced by 20mm and the height of the pole shoe should be reduced by 10mm (Figure 6 and Figure 7, λ =1.00).

This peak of the breakdown torque was further analyzed in order to obtain accurately its shape and location. This result is presented in Figure 8. Evidently, the local optimum can be reached by reducing both the pole shoe width by 20mm and the pole shoe height by 18mm.

Similar analysis is possible for every single relevant detail of the motor geometry and can be done within a relatively short CPU-time (not longer than several days on a modern multicore personal computer).

V. CONCLUSIONS

The two essentially different numerical methods the VSA and CSA for computing the torque- and current curve of SMs are presented in detail. The obtained results are verified by comparison of the two essentially different simulation tools. The obtained accuracy is excellent and more than sufficient for the daily design purposes.

The suggested numerical methodologies are relevant for modeling and simulation of the two corresponding operating modes of the adjacent cycloconverter responsible for the power supply and control of the SM.

In the paper is also demonstrated that the suggested techniques can be effectively applied for performing parameter studies and optimization of the motor geometries. Such studies are essential for revealing directions and possibilities for motor performance improvements.

REFERENCES

[1] G. Müller, B. Ponick, “Berechnung elektrischer Maschinen”, Wiley-VCH Verlag GmbH & Co., Weinheim, 2008.

[2] I. N. Grinbaum, "Calculation of no load and short circuit curves of turbo generator with nonmagnetic rotor," ELEKTROTECHNIKA, pp. 7-11, vol. 8, 1981, ENERGOIZDAT, MOSCOW.

[3] J. Jin, “The Finite Element Method in Electromagnetics”, John Wiley & Sons, Chichester, England, 1993.

[4] I. N. Grinbaum, C. Jäger, A. Fuerst, J. Smajic, “Analytical and Numerical Calculations of Synchronous Motors for Industrial Drives“, Accepted for publication at the UKSim-AMSS 8th European Modelling Symposium on Mathematical Modelling and Computer Simulation (IEEE EMS2014), Pisa, Italy, 2014.

[5] S. S. Salon, "Finite Element Analysis of Electrical Machines," Springer Science and Business Media, New York, pp. 125-158, 1995.

[6] D. A. Lowter, P.P. Silvester: Computer-Aided Design in Magnetics, Springer-Verlag, New-York, 1986.

[7] G. Müller, B. Ponick, “Grundlagen elektrischer Maschinen”, Wiley-VCH Verlag GmbH & Co KGaA, pp. 516, Weinheim, 2006.

[8] Ansys Maxwell, Commercial Electromagnetic Simulation Software, http://www.ansys.com, ANSYS Inc., 2014.

[9] MagNet v7, 2D/3D Electromagnetic Field Simulation Software, Infolytica Corp., www.infolytica.com, Montreal, Canada, 2014.